Quasiequilibrium lattice Boltzmann models with tunable bulk viscosity for enhancing stability

Quasiequilibrium lattice Boltzmann models with tunable bulk viscosity for enhancing stability

Pietro Asinari[1,*] and Ilya V. Karlin[2,3,†]
[1]*Department of Energetics, Politecnico di Torino, Corso Duca degli Abruzzi 24, Torino, Italy*
[2]*Institute of Energy Technology, ETH Zurich, 8092 Zurich, Switzerland*
[3]*School of Engineering Sciences, University of Southampton, SO17 1BJ Southampton, United Kingdom*
(Received 12 June 2009; revised manuscript received 15 November 2009; published 12 January 2010)

Taking advantage of a closed-form generalized Maxwell distribution function [P. Asinari and I. V. Karlin, Phys. Rev. E **79**, 036703 (2009)] and splitting the relaxation to the equilibrium in two steps, an entropic quasiequilibrium (EQE) kinetic model is proposed for the simulation of low Mach number flows, which enjoys both the *H* theorem and a free-tunable parameter for controlling the bulk viscosity in such a way as to enhance numerical stability in the incompressible flow limit. Moreover, the proposed model admits a simplification based on a proper expansion in the low Mach number limit (LQE model). The lattice Boltzmann implementation of both the EQE and LQE is as simple as that of the standard lattice Bhatnagar-Gross-Krook (LBGK) method, and practical details are reported. Extensive numerical testing with the lid driven cavity flow in two dimensions is presented in order to verify the enhancement of the stability region. The proposed models achieve the same accuracy as the LBGK method with much rougher meshes, leading to an effective computational speed-up of almost three times for EQE and of more than four times for the LQE. Three-dimensional extension of EQE and LQE is also discussed.

DOI: 10.1103/PhysRevE.81.016702 PACS number(s): 47.11.−j, 05.20.Dd

I. INTRODUCTION

The lattice Boltzmann (LB) method has recently met with a remarkable success as a powerful alternative for solving the hydrodynamic Navier-Stokes equations, with applications ranging from large Reynolds number flows to flows at a micron scale, porous media, and multiphase flows [1]. The LB method solves a fully discrete kinetic equation for populations $f_i(\boldsymbol{x},t)$, designed in a way that it reproduces the Navier-Stokes equations in the hydrodynamic limit in D dimensions. Populations correspond to discrete velocities $\boldsymbol{v}_i$ for $i=0,1,\ldots,Q-1$, which fit into a regular spatial lattice with the nodes $\boldsymbol{x}$. This enables a simple and highly efficient algorithm based on (a) nodal relaxation and (b) streaming along the links of the regular spatial lattice [2,3].

On the other hand, numerical stability of the LB method remains a critical issue [4]. Recalling the role played by the Boltzmann's *H* theorem in enforcing macroscopic evolutionary constraints (the second law of thermodynamics), and crediting the latter as an essential condition for enhancing the stability of the method, pertinent entropy functions have been proposed, whose local equilibrium is suitable to recover the Navier-Stokes equations [5–9].

Other heuristic methods were proposed recently in order to enhance stability of LB. The rationale behind one of them, the matrix model [10] or, equivalently, the multiple-relaxation time (MRT) [11], is to execute a collision in the moment representation (different from the propagation in the populations representation) by relaxing different moments at a different rate. Optimal relaxation can be guided by linear stability analysis [12] (even though the actual performances may be effected by the nonlinearity). Even though it was not explicitly stated in the original papers [10–12], at least a part of the enhanced stability is due to increasing the bulk viscosity of the quasicompressible LB scheme, which can be viewed as a free parameter if the incompressible flow is the only concern. Moreover, the standard lattice Bhatnagar-Gross-Krook (LBGK) method can be written as a MRT, by performing the collisions in the moment representation and, conversely, MRT can be written as a LBGK by introducing a generalized equilibrium [13]. These observations suggest that increasing the numerical bulk viscosity by itself can be considered as a leading idea and it should not be concealed by a specific way in which collisions are performed.

In this paper, we take advantage of the recent crucial result concerning the closed-form generalized equilibrium (see Eq. (3) below and Ref. [14]), in order to derive a simple entropy-based quasiequilibrium model (see [8,15,16] for a general LB setting) with tunable bulk viscosity for enhancing stability. This approach differs from the MRT, and is in fact simpler, because no collision is actually performed in any moment space, even though it is based on recognizing the role of bulk viscosity for stability enhancement. The generalized equilibrium is the analog of the anisotropic Gaussian, and is a long-needed relevant distribution in the LB method [14]. This finding allows one to derive simple LB models with an additional free-tunable parameter for controlling the bulk viscosity, where the actual range is dictated by the entropy production inequality. In addition to the preliminary results reported in Ref. [14], this paper presents details of the basic steps of construction of these models and their numerical implementation, and provides numerical examples for measuring the stability improvement.

Before going any further, let us clarify the difference between the previous approach based on the discrete-time H theorem (DTH) [6,17] and the present one based on the familiar continuous-time H theorem (CTH). In this paper, only the latter will be used, but it is important to summarize the main analogies and differences.

*pietro.asinari@polito.it
†karlin@lav.mavt.ethz.ch

The key advantage of the DTH is the notion of unconditional stability of the corresponding entropic LB scheme (the entropy function becomes a global convex Lyapunov function of the entropic LB dynamics). Moreover the positivity is automatically enforced by the condition that the H function in a postcollision state is not greater than in the precollision state. However enforcing the discrete-time H theorem comes with the need of solving a nonlinear entropy estimate at each lattice cite. The effect of the unconditional stability is the locally adaptive viscosity when the simulation is underresolved (similar to the eddy viscosity concept in large eddy simulation).

On the other hand, in the approach based on CTH theorem in the present paper, the unconditional stability is thus lost by the corresponding lattice Boltzmann time discretization. Stabilization mechanism here is not based on the DHT entropy estimate but is rather of the same nature as in the MRT models (although it is not identical to MRT as it is known in the cited literature), since the mechanism for enhancing stability is sought as increasing the bulk viscosity over the LBGK value. The CTH theorem in the present derivation is the standard one in kinetic theory (which is essentially the statement about the instantaneous entropy production inequality due to collisions), which gives a relation between the bulk and shear viscosities in this model. This is the only pertinent implication of the entropy production inequality here, it states that the bulk viscosity must be not smaller than the shear viscosity in order that the entropy production inequality remains negative, and which is consistent with the desired increase of the bulk viscosity above the shear viscosity (in LBGK they are equal). This is a simple yet useful implication of the CTH theorem (entropy production inequality), because without it the shear and bulk viscosity are only requested to be positive (but their relative magnitude is not defined) as follows from the asymptotic (Chapman-Enskog) analysis alone. The key idea is to increase the dissipation of the model for dumping the compressibility waves, which are irrelevant to the incompressible dynamics.

Summarizing, the H-function and their minimisers (equilibrium or quasiequilibria) are the same in both approaches. However these are static objects, defined irrespectively of the relaxation toward them. On the other hand, the H-theorem is always a statement about the relaxation toward these minima points, which can be differently implemented in the approaches respectively based on the DTH theorem and the CTH theorem, as shown here. The first approach ensures the unconditional stability by solving a nonlinear entropy estimate, while the second approach is much simpler but it is restricted by some stability thresholds. The interesting point is that the second approach allows one to explain clearly the link between the MRT models and the entropic models. Moreover, the CTH theorem can be used as a tool for deriving more general models on generic lattices [18].

The outline of the paper is as follows. First, for the sake of completeness, we remind the construction of continuous-time-space quasiequilibrium models, as briefly reported in Ref. [14]. In Sec. II the closed-form equilibria are discussed: in particular, in Sec. II A the generalized Maxwellian and in Sec. II B the constrained equilibrium. By means of the previous analytical results, in Sec. III the two proposed models are discussed: in Sec. III A the entropy-based model (EQE) and in Sec. III B the expanded (with regards to the local Mach number) model (LQE). The time and space discretization is done following the general procedure for quasiequilibrium LB models [8] the implementation details are reported in Sec. III C. Readers interested primarily in the practical applications can move directly to Secs. III B and III C. Numerical tests with the lid driven cavity flow are reported in Sec IV. These numerical tests suggest that the present approach is of the order of four times more efficient than the standard LBGK method with comparable accuracy. Finally, conclusions are drawn in Sec V. In the Appendix, the three-dimensional (3D) generalization of the model is presented.

II. CLOSED-FORM EQUILIBRIA

A. Generalized Maxwellian

For the sake of presentation and without any loss of generality, we consider the popular nine-velocity model, the so-called D2Q9 lattice, of which the discrete velocities are: $\boldsymbol{v}_0=(0,0)$, $\boldsymbol{v}_i=(\pm c,0)$ and $(0,\pm c)$ for $i=1-4$, and $\boldsymbol{v}_i=(\pm c,\pm c)$, for $i=5-8$ [3] where c is the lattice spacing. Recall that the D2Q9 lattice derives from the three-point Gauss-Hermite formula [19], with the following weights of the quadrature $w(-1)=1/6$, $w(0)=2/3$ and $w(+1)=1/6$. Let us arrange in the list v_x all the components of the lattice velocities along the x axis and similarly in the list v_y. Analogously let us arrange in the list f all the populations f_i. Algebraic operations for the lists are always assumed componentwise. The sum of all the elements of the list p is denoted by $\langle p\rangle=\sum_{i=0}^{Q-1}p_i$. The dimensionless density ρ, the flow velocity $\boldsymbol{u}$ and the second-order moment (pressure tensor) $\boldsymbol{P}$ are defined by $\rho=\langle f\rangle$, $\rho u_\alpha=\langle v_\alpha f\rangle$, and $\rho P_{\alpha\beta}=\langle v_\alpha v_\beta f\rangle$, respectively.

On the lattice under consideration, the convex entropy function (H function) is defined as [6]

$$H(f)=\langle f\ln(f/W)\rangle, \tag{1}$$

where $W=w(v_x/c)w(v_y/c)$. The H-function minimization problem is considered in the sequel. It is well known [6] that the equilibrium population list f_M is defined as the solution of the minimization problem $f_M=\min_{f\in\mathbf{S}_M}H(f)$, where $\mathbf{S}_M$ is the set of functions such that $\mathbf{S}_M=\{f>0:\langle f\rangle=\rho,\langle \boldsymbol{v}f\rangle=\rho\boldsymbol{u}\}$. In other words, minimization of the H function (1) under the constraints of mass and momentum conservation yields [7]

$$f_M=\rho\prod_{\alpha=x,y}w(v_\alpha/c)[2-\varphi(u_\alpha/c)]\left[\frac{2(u_\alpha/c)+\varphi(u_\alpha/c)}{1-(u_\alpha/c)}\right]^{v_\alpha/c}, \tag{2}$$

where $\varphi(z)=\sqrt{1+3z^2}$. A remarkable feature of equilibrium (2) which it shares with the ordinary Maxwellian is that it is a product of one-dimensional equilibria. In order to ensure the positivity of f_M, the low Mach number limit must be considered, i.e., $|u_\alpha|<c$.

It is possible to derive a novel constrained equilibrium, or

quasiequilibrium [20], by requiring, in addition, that the diagonal components of the pressure tensor $\boldsymbol{P}$ have some prescribed values [14]. Hence let us introduce a different minimization problem. The quasiequilibrium population list f_G is defined as the solution of the minimization problem $f_G = \min_{f \in \mathbf{S}_G} H(f)$, where $\mathbf{S}_G \subset \mathbf{S}_M$ is the set of functions such that $\mathbf{S}_G = \{f > 0 : \langle f \rangle = \rho, \langle \boldsymbol{v} f \rangle = \rho \boldsymbol{u}, \langle v_\alpha^2 f \rangle = \rho P_{\alpha\alpha}\}$. In other words, minimization of H function (1) under the constraints of mass and momentum conservation and prescribed diagonal components of the pressure tensor yields

$$f_G = \rho \prod_{\alpha=x,y} w(v_\alpha/c) \frac{3(c^2 - P_{\alpha\alpha})}{2c^2} \left(\sqrt{\frac{P_{\alpha\alpha} + cu_\alpha}{P_{\alpha\alpha} - cu_\alpha}} \right)^{v_\alpha/c} \left(\frac{2\sqrt{P_{\alpha\alpha}^2 - c^2 u_\alpha^2}}{c^2 - P_{\alpha\alpha}} \right)^{v_\alpha^2/c^2}. \tag{3}$$

To ease notation, we use $P = (P_{xx}, P_{yy})$ for a generic point on the two-dimensional plane of parameters. In order to ensure the positivity of f_G, it is required that $P \in \Omega$ where $\Omega = \{P : c|u_x| < P_{xx} < c^2, c|u_y| < P_{yy} < c^2\}$ is a convex rectangular in the plane of parameters for each velocity $\boldsymbol{u}$ (see Fig. 1).

Generalized Maxwellian (3) is the central result for the following derivations. It is interesting to note that, while equilibrium (2) is analogous to the ordinary Maxwellian (spherically symmetric Gaussian $f_M \sim \exp\{-m(\boldsymbol{v} - \boldsymbol{u})^2 / 2k_B\Theta_0\}$, shifted from the origin by the amount of mean flow velocity $\boldsymbol{u}$, and with the width proportional to the fixed temperature $\Theta_0 = c^2/3$), quasiequilibrium (3) resembles the anisotropic Gaussian, $f_G \sim \exp\{-(1/2)(\boldsymbol{v} - \boldsymbol{u}) \cdot \boldsymbol{P}^{-1} \cdot (\boldsymbol{v} - \boldsymbol{u})\}$. The latter generalized Maxwellian corresponds to the ellipsoidal symmetry, and is among the only few analytic results on the relevant distribution functions in the classical kinetic theory. It is revealing that also in the LB realm the analog of the generalized Maxwellian has a nice closed form [Eq. (3)]. We note that explicit form of the quasiequilibrium is possible due to a general result about a factorization symmetry of a certain class of quasiequilibria for discrete velocity sets established as tensor products of one-dimensional velocities (we remind that the D2Q9 velocity set is a tensor product of two copies of one-dimensional sets $\{-c, 0, c\}$; details for a general case are given in [18]).

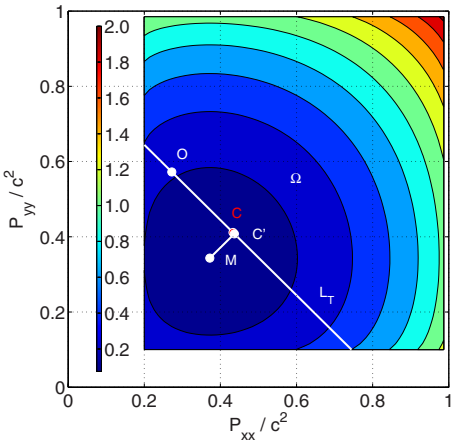

FIG. 1. (Color online) Contour plot of the entropy H_G [Eq. (4)] at $\rho = 1$, $u_x = -0.2$ and $u_y = 0.1$ ($c = 1$). Rectangular domain is the positivity domain Ω. M is the image of the Maxwellian [Eq. (2)]. O is the image of a generic nonequilibrium state while C is the image of the constrained equilibrium [Eq. (10)] (minimum of H_G on the line L_T). C' is the low Mach number approximation of C, according to approximation [Eq. (21)].

Moreover, it is possible to evaluate explicitly the H function in the generalized Maxwell states [Eq. (3)], $H_G = H(f_G)$, the result is elegantly written

$$H_G = \rho \ln \rho + \rho \sum_{\alpha=x,y} \sum_{k=-,0,+} w_k a_k(P_{\alpha\alpha}) \ln(a_k(P_{\alpha\alpha})), \tag{4}$$

where $w_\pm = w(\pm 1)$, $w_0 = w(0)$, $a_\pm(P_{\alpha\alpha}) = 3(P_{\alpha\alpha} \pm cu_\alpha)/c^2$, and $a_0(P_{\alpha\alpha}) = 3(c^2 - P_{\alpha\alpha})/(2c^2)$ (see Fig. 1).

It is worth to analyze the moments of f_G. Clearly in a discrete velocity model, the number of linearly independent moments is equal to the number of discrete velocities Q. Hence the calculation of the moments can be performed by means of a linear mapping, namely $m = Mf$, where M is the nonorthogonal transformation matrix, namely,

$$M = [1, v_x, v_y, v_x^2, v_y^2, v_x v_y, (v_x)^2 v_y, v_x (v_y)^2, (v_x)^2 (v_y)^2]^T, \tag{5}$$

which involves proper combinations of the lattice velocity components. Applying this linear mapping yields

$$m_G = M \cdot f_G = \rho[1, u_x, u_y, P_{xx}, P_{yy}, u_x u_y, u_y P_{xx}, u_x P_{yy}, P_{xx} P_{yy}]^T. \tag{6}$$

This clearly shows that the quasiequilibrium moments depend only on the constrained quantities, i.e., the conserved moments (mass and momentum) and the prescribed diagonal components of the second-order moment tensor (P_{xx} and P_{yy}). As we see, for the whole five-parametric family of functions $f_G(\rho, \boldsymbol{u}, P_{xx}, P_{yy})$ it holds that the off-diagonal component of the pressure tensor does not depend on $P_{\alpha\alpha}$, and is in the form required by the Maxwell-Boltzmann relation,

$$\langle f_G c_x c_y \rangle = \rho u_x u_y \quad \text{for any} \quad P. \tag{7}$$

The previous linear mapping M was introduced with the intent to clarify the structure of the generalized Maxwellian with regards to some meaningful moments, but this does not

effect the derivation of f_G [Eq. (3)], which is done by means of entropic concepts only. In the next section, this result is used to derive the constrained equilibrium.

B. Constrained equilibrium

With the help of f_G [Eq. (3)], let us derive a constrained equilibrium f_C which brings the H-function to a minimum among all the population lists with a fixed trace of the pressure tensor $T(\boldsymbol{P})=P_{xx}+P_{yy}$. In terms of the parameter set Ω, this is equivalent to require that the point $C=(P_{xx}^C,P_{yy}^C)$ belongs to a line segment $\mathbf{L}_T=\{P\in\Omega:P_{xx}+P_{yy}=T\}$, and the constrained equilibrium C is that minimizing the function H_G [Eq. (4)] on $\mathbf{L}_T$ (see Fig. 1). Since the restriction of a convex function to a line is also convex, the solution to the latter problem exists and is found by $[(\partial H_G/\partial P_{xx})-(\partial H_G/\partial P_{yy})]_{(P_{xx},P_{yy})\in\mathbf{L}_T}=0$, which yields a cubic equation in terms of the normal stress difference $N=P_{xx}^C-P_{yy}^C$,

$$N^3+aN^2+bN+d=0,$$

$$a=-\frac{1}{2}(u_x^2-u_y^2),\quad b=(2c^2-T)(T-u^2),$$

$$d=-\frac{1}{2}(u_x^2-u_y^2)(2c^2-T)^2. \tag{8}$$

Let us define $p=-a^2/3+b$, $q=2a^3/27-ab/3+d$, and $\Delta=(q/2)^2+(p/3)^3$. As long as $\Delta\geq 0$, which is well satisfied in the low Mach number limit, the Cardano formula implies

$$P_{xx}^C=\frac{T}{2}+\frac{1}{2}\left(r-\frac{p}{3r}-\frac{a}{3}\right),\quad r=\sqrt[3]{-\frac{q}{2}+\sqrt{\Delta}}, \tag{9}$$

while $P_{yy}^C=T-P_{xx}^C$ (note that a spurious root corresponding to $-\sqrt{\Delta}$ was neglected in Eq. (9) as it does not satisfy the asymptotics at $u_x=u_y=0$). Thus, substituting Eq. (9) into Eq. (3), we find the constrained equilibrium

$$f_C=f_G(\rho,\boldsymbol{u},P_{xx}^C(\boldsymbol{u},T),P_{yy}^C(\boldsymbol{u},T)). \tag{10}$$

Before proceeding any further, we mention that generalized Maxwellian (3) is consistent with and extends the previously known results:

(i) the point of global minimum of the function H_G [Eq. (4)] on Ω is found from $(\partial H_G/\partial P_{\alpha\alpha})=0$. The corresponding solution $M=(P_{xx}^M,P_{xx}^M)$, where $P_{\alpha\alpha}^M=-c^2/3+(2c^2/3)\sqrt{1+3(u_\alpha/c)^2}$, recovers the equilibrium f_M [Eq. (2)] upon substitution into Eq. (3): $f_M=f_G(\rho,\boldsymbol{u},P_{xx}^M(\boldsymbol{u}),P_{yy}^M(\boldsymbol{u}))$.

ii) In Ref. [8], a different LB equilibrium f_Θ was introduced as the entropy minimization problem under fixed density, momentum and energy. That equilibrium was evaluated exactly only for vanishing velocity in [8] while a series expansion was used for $\boldsymbol{u}\neq 0$. The previous result reported above solves the problem of Ref. [8] *exactly* for any velocity: Substituting $T=2\Theta+u^2$ (two-dimensional ideal-gas equation of state, with Θ the temperature) into Eq. (10), it is simply $f_\Theta(\rho,\boldsymbol{u},\Theta)=f_G(\rho,\boldsymbol{u},P_{xx}^C(\boldsymbol{u},2\Theta+u^2),P_{yy}^C(\boldsymbol{u},2\Theta+u^2))$. Expanding the exact solution P_{xx}^C [Eq. (9)] in terms of the velocity u yields the approximate solution consistent with Ref. [8], namely,

$$P_{xx}^C=\Theta+\left(\frac{\Theta+1}{4\Theta}\right)u_x^2+\left(\frac{3\Theta-1}{4\Theta}\right)u_y^2+O(\mathrm{Ma}^4). \tag{11}$$

We note that the present derivation of the exact solution at arbitrary values of $\boldsymbol{u}$ (in the definition domain) was possible due to two separate steps: First, establishing the quasiequilibrium with a factorization property, and second, by noticing that the further minimization step amounts to a simple-cubic equation. The direct minimization attempt of Ref. [8], though fully equivalent, has led to a more involved algebra which was probably the reason of overlooking the simple structure of the exact solution in that paper.

(iii) In Ref. [21], a so-called guided equilibrium $\tilde{f}_\Theta$ was introduced in order to derive LB method for compressible flows. That equilibrium is recovered by simply assuming the Maxwell-Boltzmann form of the diagonal components, $P_{xx}=\Theta+u_x^2$ and $P_{yy}=\Theta+u_y^2$, in Eq. (3): $\tilde{f}_\Theta(\rho,\boldsymbol{u},\Theta)=f_G(\rho,\boldsymbol{u},\Theta+u_x^2,\Theta+u_y^2)$.

Thus, generalized Maxwellian (3) and its implication, constrained equilibrium (10), unifies *all* the equilibria introduced previously on the D2Q9 lattice. The extension to the three dimensional case is really straightforward and the details are reported in the Appendix. Moreover, in the next section, this result is used to introduce the proposed model with tunable bulk viscosity.

III. QUASIEQUILIBRIUM KINETIC MODELS

A. Entropy-based kinetic model (EQE)

Let us introduce the entropy-based quasiequilibrium model (EQE model in the following) (see [8,15,16] for general LB setting) for the kinetic equation (time and space are both continuous)

$$\partial_t f+\boldsymbol{c}\cdot\nabla f=J(f) \tag{12}$$

where

$$J=-\frac{1}{\tau_f}(f-f_C)-\frac{1}{\tau_s}(f_C-f_M). \tag{13}$$

It is straightforward to prove the H theorem for the previous model. For that, it suffices to rewrite

$$J(f)=-\frac{1}{\tau_s}(f-f_M)-\frac{(\tau_s-\tau_f)}{\tau_f\tau_s}(f-f_C). \tag{14}$$

The entropy production $\sigma=\langle\ln(f/W)J(f)\rangle$ becomes

$$\sigma=-\frac{1}{\tau_s}\langle\ln(f/f_M)(f-f_M)\rangle-\frac{(\tau_s-\tau_f)}{\tau_f\tau_s}\langle\ln(f/f_C)(f-f_C)\rangle, \tag{15}$$

which is nonpositive $\sigma\leq 0$ and it annihilates at the equilibrium, i.e., $\sigma(f_M)=0$, provided that relaxation times satisfy the time hierarchical condition,

$$\tau_f\leq\tau_s. \tag{16}$$

Moreover, it is possible to introduce a compact form for the proposed kinetic model, namely,

$$D_t f = \partial_t f + \boldsymbol{c}\cdot\nabla f = J(f) = -\frac{1}{\tau_f}(f - f_{QE}), \tag{17}$$

where the quasiequilibrium f_{QE} is defined as

$$f_{QE}(\rho,\boldsymbol{u},T) = \frac{\tau_f}{\tau_s} f_M(\rho,\boldsymbol{u}) + \left(1 - \frac{\tau_f}{\tau_s}\right) f_C(\rho,\boldsymbol{u},T), \tag{18}$$

and it is essentially a linear interpolation between the local Maxwellian f_M and the constrained equilibrium f_C by means of the blending parameter $\tau_f/\tau_s \leq 1$. Hence the proposed model involves a quasiequilibrium with a tunable parameter (the ratio τ_f/τ_s) and it admits a H theorem as far as the free parameter is tuned such that $\tau_f/\tau_s \leq 1$. In the following, let us discuss how this parameter is related to the bulk viscosity, which is the main target of the present paper.

Recalling Eq. (14), the (truncated) moment system of equations is

$$\partial_t \rho + \partial_x(\rho u_x) + \partial_y(\rho u_y) = 0,$$

$$\partial_t(\rho u_x) + \frac{1}{2}\partial_x(\rho T) + \frac{1}{2}\partial_x(\rho N) + \partial_y(\rho P_{xy}) = 0,$$

$$\partial_t(\rho u_y) + \frac{1}{2}\partial_y(\rho T) - \frac{1}{2}\partial_y(\rho N) + \partial_x(\rho P_{xy}) = 0,$$

$$\partial_t(\rho P_{xy}) + \partial_x(\rho Q_{yxx}) + \partial_y(\rho Q_{xyy}) = -\frac{\rho}{\tau_f}(P_{xy} - u_x u_y),$$

$$\partial_t(\rho T) + \partial_x(\rho u_x) + \partial_y(\rho u_y) + \partial_x(\rho Q_{xyy}) + \partial_y(\rho Q_{yxx}) = -\frac{\rho}{\tau_s}(T - T_M),$$

$$\partial_t(\rho N) + \partial_x(\rho u_x) - \partial_y(\rho u_y) - \partial_x(\rho Q_{xyy}) + \partial_y(\rho Q_{yxx}) = -\frac{\rho}{\tau_s}(N - N_M) - \left(\frac{1}{\tau_f} - \frac{1}{\tau_s}\right)\rho(N - N_C),$$

$$\partial_t(\rho Q_{yxx}) + \partial_x(\rho P_{xy}) + \partial_y(\rho R_{xxyy}) = -\frac{\rho}{\tau_s}\left(Q_{yxx} - u_y\frac{T_M + N_M}{2}\right) - \left(\frac{1}{\tau_f} - \frac{1}{\tau_s}\right)\rho\left(Q_{yxx} - u_y\frac{T + N_C}{2}\right),$$

$$\partial_t(\rho Q_{xyy}) + \partial_x(\rho R_{xxyy}) + \partial_y(\rho P_{xy}) = -\frac{\rho}{\tau_s}\left(Q_{xyy} - u_x\frac{T_M - N_M}{2}\right) - \left(\frac{1}{\tau_f} - \frac{1}{\tau_s}\right)\rho\left(Q_{xyy} - u_x\frac{T - N_C}{2}\right),$$

$$\partial_t(\rho R_{xxyy}) + \partial_x(\rho Q_{xyy}) + \partial_y(\rho Q_{yxx}) = -\frac{\rho}{\tau_s}\left(R_{xxyy} - \frac{T_M^2 - N_M^2}{4}\right) - \left(\frac{1}{\tau_f} - \frac{1}{\tau_s}\right)\rho\left(R_{xxyy} - \frac{T^2 - N_C^2}{4}\right). \tag{19}$$

In the low Mach number limit, we have

$$N_C = u_x^2 - u_y^2 + O(\mathrm{Ma}^4), \tag{20}$$

and thus

$$N_C = N_M + O(\mathrm{Ma}^4), \tag{21}$$

where

$$N_M = \frac{2c^2}{3}\left[\sqrt{1 + 3\frac{u_x^2}{c^2}} - \sqrt{1 + 3\frac{u_y^2}{c^2}}\right] = u_x^2 - u_y^2 + O(\mathrm{Ma}^4). \tag{22}$$

Assuming the low Mach number limit and introducing the previous expression in Eq. (19), it is possible to recover approximated expressions for the nonconserved moments. In particular, the Chapman-Enskog asymptotic procedure yields the following approximations of the pressure tensor components at the leading order, indicated by the superscript (0),

$$P_{xy}^{(0)} = u_x u_y,$$

$$T^{(0)} = Dc_s^2 + u^2,$$

$$N^{(0)} = u_x^2 - u_y^2, \tag{23}$$

where $D=2$ and $c_s^2 = c^2/3$, and

$$Q_{xyy}^{(0)} = c_s^2 u_x, \quad Q_{yxx}^{(0)} = c_s^2 u_y, \tag{24}$$

for the approximations of third-order energy flux. Similarly, small deviations of the nonconserved moments from the previous approximations, indicated by the superscript [Eq. (1)], immediately follow

$$P_{xy}^{(1)} = -\tau_f c_s^2(\partial_y u_x + \partial_x u_y),$$

$$T^{(1)} = -\tau_s D c_s^2(\partial_x u_x + \partial_y u_y),$$

$$N^{(1)} = -\tau_f D c_s^2(\partial_x u_x - \partial_y u_y). \tag{25}$$

Grouping together leading-order approximations, i.e., $P_{xy}^{(0)}$, $T^{(0)}$, and $N^{(0)}$ given by Eq. (23), and small deviations of the nonconserved moments, i.e., $P_{xy}^{(1)}$, $T^{(1)}$, and $N^{(1)}$ given by Eq. (25), allows one to recover the hydrodynamic equations

$$\partial_t \rho + \partial_\alpha(\rho u_\alpha) = 0,$$

$$\partial_t u_\alpha + u_\beta\partial_\beta u_\alpha + \frac{1}{\rho}\partial_\alpha(c_s^2\rho) - \frac{1}{\rho}\partial_\beta\left[\nu\rho\left(\partial_\alpha u_\beta + \partial_\beta u_\alpha - \frac{2}{D}\delta_{\alpha\beta}\partial_\gamma u_\gamma\right)\right] - \frac{1}{\rho}\partial_\alpha(\xi\rho\partial_\gamma u_\gamma) = 0, \tag{26}$$

where the transport coefficients are

$$\nu = \tau_f c_s^2, \quad \xi = \tau_s c_s^2, \tag{27}$$

for the kinematic viscosity and the bulk viscosity, respectively. Thus, from [Eq. (16)], the bulk viscosity is larger than the kinematic viscosity in this model,

$$\nu \leq \xi. \tag{28}$$

In particular, the parameter for enhancing stability is the ratio $\xi/\nu \geq 1$, as pointed out by the following numerical tests. Before proceeding with the numerical implementation, the next section reports a simplified version of the model, based on expansion with regards to the low Mach number limit.

B. Expanded model (LQE)

The goal of this section is to provide the basic details of a simplified version of the kinetic model, based on the expansion with regards to the Mach number (LQE model in the following). The simplification concerns the following three issues:

(i) first of all, recalling the compact form given by Eq. (18), it is possible to realize that the proposed quasiequilibrium f_{QE} requires to compute twice the same generalized Maxwellian f_G with different arguments, namely,

$$f_{QE}(\rho,\boldsymbol{u},T) = \frac{\tau_f}{\tau_s} f_G(\rho,\boldsymbol{u},P_{xx}^M(\boldsymbol{u}),P_{yy}^M(\boldsymbol{u})) + \left(1-\frac{\tau_f}{\tau_s}\right) f_G(\rho,\boldsymbol{u},P_{xx}^C(\boldsymbol{u},T),P_{yy}^C(\boldsymbol{u},T)). \tag{29}$$

(ii) Second, the generalized Maxwellian f_G given by Eq. (3) with generic arguments (P_{xx},P_{yy}) can be expressed in a simpler equivalent way in terms of components, namely,

$$f_{G(0,0)} = \frac{\rho}{c^4}(c^2-P_{xx})(c^2-P_{yy}),$$

$$f_{G(\pm 1,0)} = \frac{\rho}{2c^4}(P_{xx} \pm cu_x)(c^2-P_{yy}),$$

$$f_{G(0,\pm 1)} = \frac{\rho}{2c^4}(c^2-P_{xx})(P_{yy} \pm cu_y),$$

$$f_{G(\pm 1,\pm 1)} = \frac{\rho}{4c^4}(P_{xx} \pm cu_x)(P_{yy} \pm cu_y). \tag{30}$$

(iii) Finally, in the low Mach number limit, recalling that $P_{\alpha\alpha}^M = -c_s^2 + 2c_s^2\sqrt{1+u_\alpha^2/c_s^2}$ and recalling Eq. (20), the following expressions:

$$P_{xx}^M(\boldsymbol{u}) = c_s^2 + u_x^2 + O(\mathrm{Ma}^4),$$

$$P_{yy}^M(\boldsymbol{u}) = c_s^2 + u_y^2 + O(\mathrm{Ma}^4), \tag{31}$$

hold for the equilibrium moments, while the expressions

$$P_{xx}^C(\boldsymbol{u},T) = \frac{T}{2} + u_x^2 - \frac{u_x^2+u_y^2}{2} + O(\mathrm{Ma}^4),$$

$$P_{yy}^C(\boldsymbol{u},T) = \frac{T}{2} + u_y^2 - \frac{u_x^2+u_y^2}{2} + O(\mathrm{Ma}^4), \tag{32}$$

hold for the constrained moments, where the residuals $O(\mathrm{Ma}^4)$ can be neglected in both cases. Equations (30) and (32) are generalized for the three-dimensional case in the Appendix.

It should be stressed that, while the results for the EQE model are exact for any $\boldsymbol{u}$ (subject to the positivity constraint), the later restriction to the low Mach number expansion is a matter of convenience, and it leaves intact the overall accuracy (with respect to recovering hydrodynamic equations) of the proposed model. We concluded this section by pointing out the connection between the expanded model and the multiple-relaxation-time (MRT) collision operator [14]. First of all, as far as the hydrodynamic limit is concerned, the deviations of quasiequilibrium moments from equilibrium values can be neglected for all orders strictly higher than the second. In other words, for third and fourth order moments, the equilibrium values can be substituted instead of the quasiequilibrium values, without effecting the leading hydrodynamics. Hence it remains to discuss the second-order deviations. Combining the expressions given by Eqs. (32) yields

$$P_{xx}^C(\boldsymbol{u},T) = \frac{P_{xx}+P_{yy}+P_{xx}^M-P_{yy}^M}{2},$$

$$P_{yy}^C(\boldsymbol{u},T) = \frac{P_{xx}+P_{xx}-P_{xx}^M+P_{yy}^M}{2}. \tag{33}$$

Recalling Eqs. (17) and (29), the second-order deviations become

$$P_{xx}^{QE}-P_{xx} = \frac{\beta+1}{2}(P_{xx}^M-P_{xx}) + \frac{\beta-1}{2}(P_{yy}^M-P_{yy}),$$

$$P_{yy}^{QE}-P_{yy} = \frac{\beta-1}{2}(P_{xx}^M-P_{xx}) + \frac{\beta+1}{2}(P_{yy}^M-P_{yy}), \tag{34}$$

where $\beta = \tau_f/\tau_s \leq 1$. Taking into account the previous expressions, the collision operator can be approximated by

$$J'(f) = -A(f-f_M), \tag{35}$$

where $A = 1/\tau_f M^{-1}\Lambda M$, M is the linear mapping defined by Eq. (5) and the 9×9 matrice Λ is

$$\Lambda = \mathrm{diag}\left([1,1,1],\begin{bmatrix}\beta_+ & \beta_- \\ \beta_- & \beta_+\end{bmatrix},[1,1,1,1]\right), \tag{36}$$

with $\beta_\pm = (\beta \pm 1)/2$. Operator J' is a collision operator in a matrix form [4] with collision matrix A (characterized by two relaxation times τ_f and $\tau_f/\beta = \tau_s$), but it can be easily expressed as a MRT collision integral [22], by using the mapping M for defining a moment representation.

In the next section, some details are reported concerning the numerical implementation in order to avoid the discrete lattice effects, i.e., numerical errors due to the spatial discretization (lattice Knudsen number), which may effect the expressions of the effective transport coefficients.

C. Lattice Boltzmann realization

Let us derive a lattice Boltzmann scheme from the kinetic model, Eqs. (17) and (18), following the general procedure of Ref. [8]. Kinetic Eq. (17) is integrated in time from t to $t+\delta t$ along characteristics, and the time integral of the right-hand side is evaluated by trapezoidal rule to get

$$f(\boldsymbol{x}+\boldsymbol{v}\delta t,t+\delta t)-f(\boldsymbol{x},t)=\frac{\delta t}{2}J(f(\boldsymbol{x}+\boldsymbol{v}\delta t,t+\delta t))+\frac{\delta t}{2}J(f(\boldsymbol{x},t)). \tag{37}$$

The latter expression involves implicit computations, which may be cumbersome to code. In order to avoid them, let us apply the following variable transform [8,23]:

$$f\rightarrow g=f-\frac{\delta t}{2}J(f), \tag{38}$$

to Eq. (37), which yields

$$g(\boldsymbol{x}+\boldsymbol{v}\delta t,t+\delta t)=(1-\omega_f)g(\boldsymbol{x},t)+\omega_f f_{QE}(\rho,\boldsymbol{u},T_{CN}), \tag{39}$$

where $\rho=\langle g\rangle$ and $\boldsymbol{u}=\langle \boldsymbol{v}g\rangle/\langle g\rangle$, because mass and momentum are conserved, while

$$T_{CN}(g)=\left(1-\frac{\omega_s}{2}\right)T(g)+\frac{\omega_s}{2}T_M(g), \tag{40}$$

$$T(g)=\langle (v_x^2+v_y^2)g\rangle, \tag{41}$$

$$T_M(g)=\frac{2c^2}{3}\left[\sqrt{1+3\frac{u_x^2}{c^2}}+\sqrt{1+3\frac{u_y^2}{c^2}}-1\right]=\frac{2c^2}{3}+u_x^2+u_y^2+O(\mathrm{Ma}^4), \tag{42}$$

and

$$\omega_f=\frac{2\delta t}{2\tau_f+\delta t},\quad \omega_s=\frac{2\delta t}{2\tau_s+\delta t}. \tag{43}$$

In particular, using the first or the second expression reported in Eq. (42) depends on the considered model, i.e., if the entropy-based model or the expanded model is implemented respectively. By means of Chapman-Enskog asymptotic procedure, it is possible to prove that the previous lattice Boltzmann scheme recovers the Navier-Stokes equations up to the second order with regards to $\delta x=c\,\delta t$, with the kinematic viscosity $\nu=\tau_f c_s^2$ and the bulk viscosity $\xi=\tau_s c_s^2$, as it happens for the continuous (in space and time) kinetic model.

A few comments on the above discretization scheme are in order. First, we remark that a simpler discretization of kinetic equation using a forward Euler scheme, $f(\boldsymbol{x}+\boldsymbol{v}\delta t,t+\delta t)-f(\boldsymbol{x},t)=\delta t J(f(\boldsymbol{x},t))$ is only first-order accurate in the above sense. For $\tau_s=\tau_f$ (that is, for the BGK case), the latter scheme can be reinterpreted as a second-order accurate with rescaled viscosity coefficients, as is well known. However, in general, such a reinterpretation is not straightforward if collision integral depends explicitly on the nonconserved moments (or, in other words, it depends explicitly on a quasiequilibrium distribution rather than solely on the local equilibrium). This is the situation at hand when $\tau_f<\tau_s$. Therefore, in order to avoid the reinterpretation step (which is somewhat arbitrary), we used a general method for quasiequilibrium models available in the literature [8]. Second, the above scheme should not be confused with the entropic time stepping scheme (or the discrete-time H theorem) [5–9]. In the latter case, the entropy estimate of the collision step is applied after every advection step which guarantees the nonincrease of the H function. In the present case, the continuous-time H theorem established above delivers the estimate for the parameters of the model (the relaxation times τ_f and τ_s), while the discrete-time H theorem is not implemented by scheme (39). Finally, both the methods [5–9] and the present one define equilibria and quasiequilibria as a minimum of the pertinent entropy function under corresponding constraints, with a further optional simplification at low Mach numbers.

In the next section, some numerical tests are reported in order to prove the effectiveness of the proposed scheme with enhanced stability.

IV. NUMERICAL VALIDATION BY LID DRIVEN CAVITY

The proposed scheme with enhanced stability has been already preliminary tested in Ref. [14] by means of the Taylor-Green vortex flow, in order to prove that even large bulk viscosities may be adopted without affecting significantly the numerical results at low Mach numbers. In this section, the effective enhanced stability is measured for the two-dimensional lid driven cavity test, and a relation between stability and accuracy is established. This test has been chosen because it is characterized by singularity of the pressure in the lid corners and hence it is suitable for testing the robustness of the scheme. In the following sections, the enhanced stability is investigated first and then the relation with the accuracy in terms of both vortex locations and global solution is studied.

A. Stability test

Let us solve the standard lid driven cavity flow by using the proposed entropic quasiequilibrium model. Let us consider a square domain $(x,y)\in[0,L]\times[0,L]$ and let us assume $L=1$. Moreover the simulation time is $t\in[0,t_0]$, where $t_0=100$, which is considered enough to reach the steady-state conditions for the considered Reynolds numbers (see next). The computational domain is discretized by a uniform collocated grid with $N\times N$ points. The boundaries are located half cell away from the computational nodes. Let us denote $\boldsymbol{x}_b$ the generic boundary computational node. Clearly, in all inner computational nodes ($\boldsymbol{x}\neq\boldsymbol{x}_b$), Eq. (39) holds for any lattice velocity $\boldsymbol{v}_i$. In the generic boundary computational node $\boldsymbol{x}_b$, Eq. (39) holds for any lattice velocity $\boldsymbol{v}_i$ such that $\boldsymbol{x}_b+\boldsymbol{v}_i\delta t$ is still a computational node. In case $\boldsymbol{x}_b+\boldsymbol{v}_i\delta t$ is out of the computational grid, then the following boundary condition holds

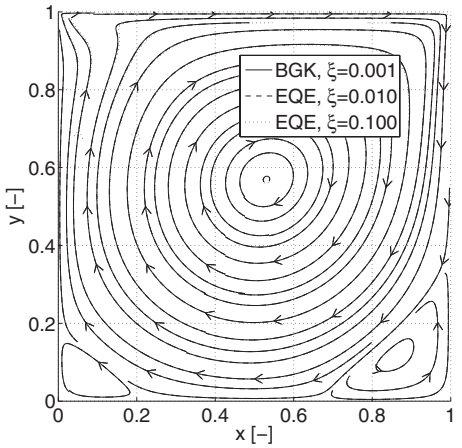

FIG. 2. Streamlines for the lid driven cavity flow with Re $=1000$, $t_0=100$ and mesh 160×160. The kinematic viscosity is fixed to $\nu=0.001$, while different values of the bulk viscosities $\xi \in [0.001, 0.1]$ are considered, where $\xi=0.001$ corresponds to the single relaxation-time BGK case ($\xi=\nu$).

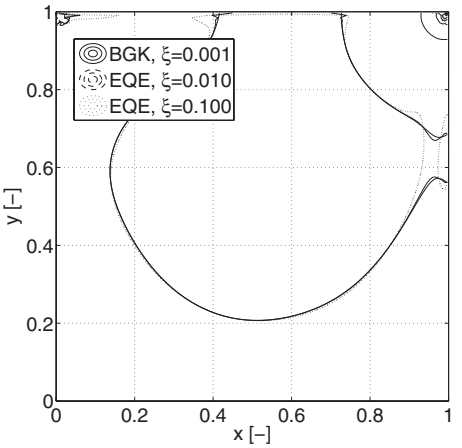

FIG. 3. Pressure field contours for the lid driven cavity flow with Re$=1000$, $t_0=100$ and mesh 160×160. The kinematic viscosity is fixed to $\nu=0.001$, while different values of the bulk viscosities $\xi \in [0.001, 0.1]$ are considered.

$$g_{\bar{i}}^{*}(\boldsymbol{x}_b, t+\delta t) = g_i^{*}(\boldsymbol{x}_b, t) - 6 f_M(\rho, \boldsymbol{0}) \boldsymbol{v}_i \cdot \boldsymbol{u}_b / c^2, \qquad (44)$$

where $\boldsymbol{v}_{\bar{i}}=-\boldsymbol{v}_i$ is the bounce-back lattice velocity, $g^*(\boldsymbol{x},t)$ is the postcollision distribution function defined as

$$g^{*}(\boldsymbol{x},t) = (1-\omega_f) g(\boldsymbol{x},t) + \omega_f f_{QE}(\rho, \boldsymbol{u}, T_{CN}), \qquad (45)$$

and $\boldsymbol{u}_b$ is the boundary velocity (imposed half cell away from the boundary computational node $\boldsymbol{x}_b$). In the following numerical simulations, $\boldsymbol{u}_b=(u_L,0)^T$ at the lid wall, where u_L is the lid velocity, and $\boldsymbol{u}_b=\boldsymbol{0}$ for all the other walls. At the lid corners, the lid velocity is imposed, while for other corners the boundary conditions given by Eq. (44) are composed.

Since we are interested in the incompressible limit, the effect of the bulk viscosity ξ, considered as a free tunable parameter, is analyzed. In Figs. 2 and 3, the numerical results are reported for the case of Reynolds number $\mathrm{Re}=u_L L/\nu=1000$. Concerning the streamlines, it is confirmed that even large ratios of ξ/ν does not practically effect the result. However the limit on the pressure field is more strict because beyond $\xi/\nu=10$ some slight effects on the pressure contours are found. Hence in the following, the bulk viscosity is fixed to $\xi=10\nu$.

First of all, let us analyze the pure stability enhancement of the proposed model. It is well known that, the lid driven cavity involves a singular pressure field, in the top lid corners of Fig. 3. For this reason, this numerical test is well suited for checking the actual stability of a numerical scheme in dealing with nonlinear Navier-Stokes equations. In particular, the singular pressure corners excite and promote compressible waves in the pressure field. The key of the entropic quasiequilibrium is to use large bulk viscosity to damp this pressure waves and attenuate them effectively. As reported in Table I, this attenuation mechanism leads to a consistent enhancement of the stability performance of the scheme. Practically this means that the proposed scheme can deal with much smaller meshes (essentially one fourth of the minimum mesh required by the usual BGK scheme).

Introducing the Mach number $\mathrm{Ma}=u_L/c$, where u_L is the lid velocity and c is the lattice speed, recalling that $c_s=c/\sqrt{3}$ and $\nu=\tau_f c_s^2$, and using the definition of the Reynolds

TABLE I. Lid driven cavity stability test. Some numerical tests are reported for different kinematic viscosity ν (and consequently Reynolds number Re) for both standard BGK and proposed entropic quasiequilibrium model (EQE). The bulk viscosity is fixed to $\xi=10\nu$ and it is a pure numerical artifact. The minimum number min(N) of points along each coordinate for running stable simulations is reported. The latter corresponds to the maximum Mach number tolerated by the numerical scheme, namely max (Ma), where $\mathrm{Ma}=u_L/c$, u_L is the lid velocity, and c is the lattice speed. In the numerical simulations, $\mathrm{Ma}=0.01$ Re Kn is adopted.

		BGK $\xi=\nu$			EQE$\xi=10\nu$		
Re	ν	Min (N)	Max (Ma)	Max (Kn)	Min (N)	Max (Ma)	Max (Kn)
1000	1.0×10^{-3}	50	0.2	0.0200	25	0.4	0.0400
2000	5.0×10^{-4}	100	0.2	0.0100	50	0.4	0.0200
3000	3.3×10^{-4}	150	0.2	0.0067	75	0.4	0.0133
4000	2.5×10^{-4}	200	0.2	0.0050	100	0.4	0.0100
5000	2.0×10^{-4}	250	0.2	0.0040	125	0.4	0.0080

number $\mathrm{Re}=u_L L/\nu$, it is possible to derive the following relation (analogous to the von Karman relation):

$$\mathrm{Ma}=\frac{\tau}{3\delta t}\mathrm{Re}\ \mathrm{Kn}, \tag{46}$$

where $\mathrm{Kn}=\delta x/L=1/N$ and N is the number of grid points along length L (the lattice Knudsen number). From the asymptotic analysis of the LB model based on the assumption that both Kn and Ma are small, it is possible to prove that there are two terms in the recovered macroscopic equations, in addition to those prescribed by the incompressible Navier-Stokes equations, which are respectively $O(\mathrm{Kn}^2)$ and $O(\mathrm{Ma}\ \mathrm{Kn})$ [24]. Hence, two strategies are possible. In case one wants to obtain a second-order numerical method with regards to the space resolution, i.e., with regards to Kn, taking into account Eq. (46), $\mathrm{Ma}\sim\mathrm{Kn}$ must be selected, which means $\tau_f/\delta t\sim O(1)$, or equivalently keeping $\tau_f/\delta t$ fixed on different meshes. The latter corresponds to the so-called diffusive (or parabolic) scaling. On the other hand, in case of advective (or hyperbolic) scaling, one wants to keep Ma independent of lattice Kn, then τ_f becomes constant independent of the considered mesh. Below we use diffusive scaling when setting up the parameters of various simulations.

In particular, in Table I, since Ma/Kn becomes a constant in the diffusive scaling, then any (stability and/or accuracy) constraint on $\mathrm{Kn}=1/N$ can be formulated also in terms of Ma. Hence in Table I, the enhancement of the stability performance of the scheme can also be expressed as the ability to deal with much larger Mach numbers, i.e., to perform much faster simulations. Obviously in this case, deviations from the Maxwell-Boltzmann equilibrium may spoil the accuracy of the numerical solutions.

Concerning the latter point, it is worth the effort to point out that the stability threshold appears quite earlier than the non-negativity condition for the generalized population list. Recalling the definition given by Eq. (3), it is easy to derive the positivity condition as $\mathrm{Ma}\leq\sqrt{2/3}\approx 0.8165$. However the instability for EQE model appears at roughly $\mathrm{Ma}=0.4$. This means that, at least for the present test case, the stability region fits well into the non-negativity region, where the generalized Maxwellian given by Eq. (3) is defined.

B. Stability and accuracy test with regards to vortex locations

Clearly a fair comparison among the numerical schemes should take into account the actual accuracy as well. In fact, improving the bulk viscosity may allows one to adopt rougher meshes but reducing the recovered accuracy. In order to check this, let us consider the case $\mathrm{Re}=5000$. For this Reynolds number, it is well known that four main vortexes appear in the lid driven cavity, namely, upper-left (U-L), mid-central (M-C), lower-left (L-L), and lower-right (L-R), see Fig. 4. It is possible to compute the actual "centers" of the vortexes as the local extrema of the stream function ψ, defined as

$$u_x=\frac{\partial\psi}{\partial y},\quad u_y=-\frac{\partial\psi}{\partial x}. \tag{47}$$

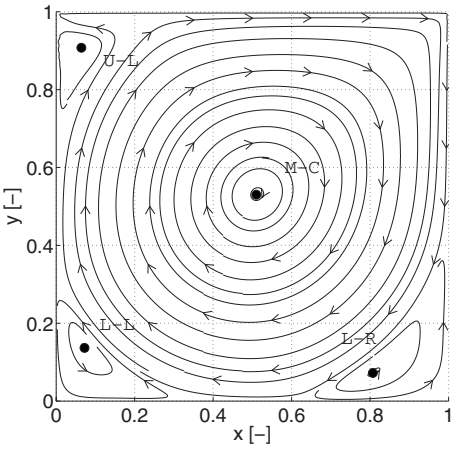

FIG. 4. Streamlines for the lid driven cavity flow with $\mathrm{Re}=5000$, $t_0=100$ and mesh 150×150. The kinematic viscosity is fixed to $\nu=0.0002$, while the bulk viscosity to $\xi=0.002$. Four main vortexes appear: upper-left (U-L), mid-central (M-C), lower-left (L-L) and lower-right (L-R).

Let us consider previous calculations concerning the locations of the main vortexes [25–28]. Let us define $\boldsymbol{x}_q=(x_q,y_q)^T$ the vector which locates the center of the vortex q, where $q\in[\mathrm{U\text{-}L},\mathrm{M\text{-}C},\mathrm{L\text{-}L},\mathrm{L\text{-}R}]$. Clearly there is no perfect agreement among the previous references about the vortex locations. Hence in the following, we consider the reference values $\boldsymbol{x}_q^r$ as the (arithmetic) average of the values reported in each of the four references [25–28].

Another problem is related to the effect of the adopted mesh. If one forces the calculation of the vortex location to be limited only to the nodes of the adopted mesh, the final accuracy will depends on both the accuracy of the numerical velocity field and on the constraint of the available discrete nodes. Hence the rough meshes are penalized twice. However the first issue is relevant while the second is actually an overconstraint which can be avoided. In fact, in the following calculations, all the numerical velocity fields (coming from the numerical scheme with different meshes) are interpolated first on the same finer mesh, then the vortex location is searched for on the finer mesh (by a standard tool for locating the extrema of the stream function). In this way, even though the calculations are performed with different meshes, the final output after postprocessing, in terms of vortex location, is produced with the same discrete grid. The latter postprocessing step makes all the simulations fairly comparable with each other. The postprocessing is composed of the following steps: interpolation on the finer mesh, computation of the stream function and location of the extrema of the stream function, which are actually the vortex locations.

Let us denote $\boldsymbol{x}_q$ the location of the vortex q, according to the adopted numerical scheme and after postprocessing. Hence it is possible to introduce the following errors: the vortex error E_q for the qth vortex, namely,

$$E_q=\frac{\|\boldsymbol{x}_q-\boldsymbol{x}_q^r\|}{\|\boldsymbol{x}_q^r\|}, \tag{48}$$

where $\|\cdot\|$ is the L_2-norm and E_m is the (arithmetic) mean error. In Table II, the results of the numerical simulations are

TABLE II. Lid driven cavity stability and accuracy test. The Reynolds number is Re=5000, the kinematic viscosity ν=0.0002 and the bulk viscosity ξ=0.002. Different meshes are considered. For each numerical calculation, the locations of the four main vortexes (see Fig. 4) are computed by postprocessing on the same finer mesh 250×250 and compared with some reference values [25–28]. The error on the location of each vortex q, namely, E_q, is computed by Eq. (48), while E_m is the arithmetic average among all the errors. All the models were run on same hardware. Actual run time is normalized to the run time taken by the EQE model on the 170×170 grid.

			Vortex locations				Errors on vortex locations (%)				
	Run time	Axis	M-C	L-L	L-R	U-L	M-C	L-L	L-R	U-L	Mean
References [25–28]	NA	x_q^r	0.51393333	0.07040000	0.82213333	0.06460000	0.00	0.00	0.00	0.00	0.00
		y_q^r	0.53460000	0.14343333	0.07666667	0.90805000					
EQE 125×125	0.35	x_q	0.51004016	0.07630522	0.81124498	0.05220884	1.15	12.41	1.61	1.36	4.13
		y_q	0.54216867	0.12449799	0.08433735	0.90763052					
EQE 150×150	0.61	x_q	0.51807229	0.07630522	0.80321285	0.06425703	0.74	12.41	2.29	0.49	3.98
		y_q	0.53815261	0.12449799	0.07630522	0.90361446					
EQE 170×170	1.00	x_q	0.52208835	0.07228916	0.80321285	0.06508876	1.20	6.93	2.29	0.30	2.68
		y_q	0.53815261	0.13253012	0.07630522	0.90532544					
LQE 170×170	0.65	x_q	0.51004016	0.07228916	0.80722892	0.06425703	0.80	4.47	1.88	0.06	1.80
		y_q	0.53012048	0.13654618	0.07228916	0.90763052					
EQE 200×200	2.06	x_q	0.52208835	0.06827309	0.80722892	0.06425703	1.10	4.51	1.81	0.06	1.87
		y_q	0.53413655	0.13654618	0.07630522	0.90763052					
EQE 250×250	4.97	x_q	0.52208835	0.06827309	0.80321285	0.06425703	1.10	2.24	2.35	0.06	1.44
		y_q	0.53413655	0.14056225	0.07228916	0.90763052					
ELB[a] 320×320	NA	x_q	0.51750000	0.07730000	0.80560000	0.06640000	0.48	6.35	2.09	0.22	2.29
		y_q	0.53500000	0.13600000	0.07160000	0.90900000					
BGK 250×250	2.84	x_q	0.51807229	0.07630522	0.80722892	0.06425703	1.16	7.76	1.88	0.06	2.72
		y_q	0.54216867	0.13253012	0.07228916	0.90763052					

[a]Reference [29].

reported. Essentially for the present test, EQE model is able to deal with a very coarse mesh 125×125, which is roughly one fourth of the minimum mesh for the BGK model, namely, 250×250. However, in terms of accuracy, this coarse mesh is not able to produce the same performance for computing the vortex locations, even though the numerical velocity field is interpolated on the same fine mesh. Hence the mesh of the EQE must be refined. It comes out that the EQE model, with a rougher mesh $170^2 \sim 250^2/2$ than that used by the BGK model, can achieve similar accuracy (2.68%~2.72%). In Fig. 5, the locations of the main vortexes computed by both EQE and BGK are reported and compared with the reference values. Hence if both stability and accuracy are concerned, the EQE model can deal with one half of the mesh required by the BGK model. This advantage can compensate the additional computational overhead of the EQE model and it leads to an effective computational speed-up for EQE model of 2.84 times over the BGK model. In other words, even though more calculations are required in each cell because of the Cardano analytical formula, the reduced number of cells is at the end still the leading advantage. It is not surprising that EQE can achieve better accuracy with rougher meshes. In fact the errors are due mainly to the compressible waves traveling in the domain. Since the BGK model with 250×250 mesh is still quite close to the stability threshold, it is clear that the compressibility waves are still relevant there, more than what happens for the EQE model which is able to effectively damp them.

Finally, in Table II, the results obtained by the expanded model in the low Mach number limit (LQE) are reported as well for the mesh 170×170. First of all, the LQE model is roughly 50% faster than the EQE model, because the former avoids the cumbersome calculations due to the Cardano formula. Moreover, it is even more accurate than the full

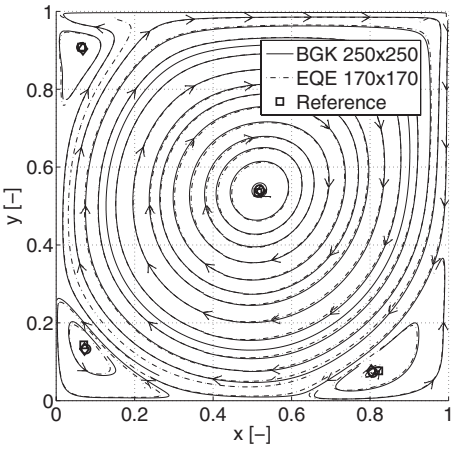

FIG. 5. Streamlines for the lid driven cavity flow with Re =5000, ν=0.0002 (ξ=0.002 for the EQE model only). The reference locations $\boldsymbol{x}_q^r$ for the four main vortexes are reported [25–28] (square markers). Moreover the computed locations $\boldsymbol{x}_q$ based on the postprocessing are reported too for both BGK (circle markers) and EQE model (diamond markers).

entropy-based model (1.80% < 2.68%), because it involves a smaller number of operations and hence it is less effected by the round-off errors. It is worth to recall that the difference between LQE and EQE is $O(\mathrm{Ma}^4)$, i.e., it is 2 orders of magnitude smaller than the accuracy of the numerical scheme in case of diffusive scaling, when the Mach number is selected proportional to the Knudsen number. For these reasons, use of LQE in practical simulations is recommended, even though more test cases need to be studied.

C. Stability and accuracy test with a global solution

Even though the computation of the vortex locations is a standard procedure for checking the accuracy of the considered numerical scheme, we also compared globally the recovered solutions with a reference solution. The computational domain and the physical parameters are identical to those considered in the previous section, i.e., $L=1$, $t_0=100$, $\nu=0.0002$, $\xi=10\nu$ (for EQE and LQE), $u_L=1$, $\mathrm{Re}=5000$.

The reference solution has been obtained by means of a commercial computational fluid-dynamics (CFD) code FLUENT®, based on the finite-volume method (FVM), which is a quite popular tool in computational engineering. First of all, the reference solution was computed by using double precision representation, i.e., binary floating-point number format using 64 bits, for reducing the effects of the machine round-off precision. Concerning the spatial discretization, the second-order up-wind was considered for the discretization of the momentum fluxes. For the resolution of the discrete equations, a segregated approach was used; i.e., the continuity and momentum equations were solved alternatively by means of an iterative solution up to convergence. The SIMPLEC algorithm [30] was used for the pressure-velocity coupling: essentially this algorithm is used to solve the Poisson equation coming out by combining the momentum equation with the divergence-free condition for the low Mach number limit. As a convergence criterion, it was required that all the residuals are smaller than 10^{-7}, i.e., the imbalances in all the discretized equations summed over all the computational cells are smaller than 10^{-7} during the final convergence step. The reference solution is indicated by $(u_x^r, u_y^r, p^r)(x,y)$, where u_x^r, u_y^r are the velocity components, p^r is the pressure and $\boldsymbol{x}=(x,y)^T \in G(N)$ with $G(N)$ meaning the computational grid made of $N \times N$ homogeneously spanned (collocated) computational nodes. The values on the collocated grid are computed by interpolation because the commercial code uses a staggered grid (as popular for avoiding checkerboard instability in FVM). In particular, the grid 1025×1025 was used for computing the reference solution in the following calculations. The actual reference for a rougher mesh $N<1025$ was obtained by means of bicubic interpolation, i.e., cubic interpolations along both Cartesian axes.

In order to characterize properly the behavior of the proposed schemes, an extensive simulation plan has been defined. The Knudsen number, i.e., the spatial resolution, was selected such that $\mathrm{Kn} \in \{1/128, 1/160, 1/192, 1/224, 1/256\}$ (linearly spanned), or equivalently the computational nodes along each Cartesian axis was selected such that $N \in \{128, 160, 192, 224, 256\}$. Taking into account Eq. (46) and adopting the diffusive scaling, the Mach number was tuned by means of the constant $\tau_f/\delta t$, which must be mesh independent. In particular, the Mach number was selected such that $\mathrm{Ma} \in \{0.02, 0.04, 0.1, 0.2, 0.4\}$ (roughly logarithmically spanned). Finally, for each combination of the previous parameters, three schemes were tested: the standard lattice BGK, EQE, and LQE. This leads to a simulation plan made of a total $5 \times 5 \times 3 = 75$ runs.

The global errors were computed for different meshes, namely,

$$E_{ux} = \frac{1}{u_L}\sqrt{\frac{1}{N^2}\sum_{\boldsymbol{x}\in G(N)}(u_x - u_x^r)^2}, \tag{49}$$

$$E_{uy} = \frac{1}{u_L}\sqrt{\frac{1}{N^2}\sum_{\boldsymbol{x}\in G(N)}(u_y - u_y^r)^2}, \tag{50}$$

$$E_p = \frac{1}{u_L^2}\sqrt{\frac{1}{N^2}\sum_{\boldsymbol{x}\in G(N)}(p - p^r)^2}, \tag{51}$$

where the pressure $p=c_s^2(\rho-\rho_0)$ has been normalized in order to have the same mean of the reference solution p^r. The numerical results are reported in Table III. First of all, it is not surprising that an unstable behavior may appear for low values of the Mach number. In fact, recalling Eq. (46), the quantity $\tau_f/\delta t$ (mesh independent under the diffusive scaling), namely,

$$\frac{\tau_f}{\delta t} = 3\frac{\mathrm{Ma}}{\mathrm{Re}\,\mathrm{Kn}}, \tag{52}$$

becomes small when the Mach number is small. Consequently, taking into account Eq. (43), ω_f tends to 2, which is the upper stability threshold for the evolution Eq. (39), in terms of transformed distribution function g. Comparing different numerical schemes, EQE and LQE show a wider stability region since these schemes allow one to consider quite rough meshes up to $N=128$, while the standard BGK requires at least $N=256$. Moreover, EQE is characterized by better accuracy in recovering the global solution than LQE and, as expected, the discrepancy between these schemes increases as long as the Mach number increases. Considering the EQE scheme, it is possible to recover the same mean accuracy of the best lattice BGK simulation ($1/\mathrm{Kn}=256$ and $\mathrm{Ma}=0.20$), i.e., $E_m=1.2\%$, by using a rougher mesh with $1/\mathrm{Kn}=192$ and $\mathrm{Ma}=0.20$, which corresponds roughly to half of the previous mesh.

Finally, it is interesting to analyze the mean errors for EQE on the parameter plane given by (Kn, Ma), as reported in Table IV, where the best results are shown in bold. For any mesh, i.e., for any numerical Knudsen number, there is an optimal Mach number which yields the most accurate results. Larger Mach numbers tend to violate the assumption used to derive the discrete local equilibrium, while smaller Mach numbers yield smaller dimensionless viscosities expressed in lattice units, which lead to more inaccurate numerical results. This optimal Mach number slightly increases for rougher meshes. The above systematic simulation plan

TABLE III. Lid driven cavity stability and global accuracy test. The Reynolds number is Re=5000, the kinematic viscosity ν=0.0002 and the bulk viscosity ξ=0.002 (for EQE and LQE). Different meshes (and consequently different Knudsen numbers) $N=1/\mathrm{Kn}$ and different Mach numbers are considered. The global errors on the velocity components E_{ux} and E_{uy} and on pressure E_p are computed by Eq. (49), while E_m is the arithmetic average among all the previous errors. The label "unstable" means that the calculation could not be performed with that combination of simulation parameters.

			Ma				
1/Kn	Scheme	Error	0.02	0.04	0.10	0.20	0.40
128	BGK				Unstable		
	EQE	E_{ux}		Unstable	0.024998	0.019096	0.021838
		E_{uy}		Unstable	0.025482	0.019629	0.021678
		E_p		Unstable	0.022485	0.013274	0.008023
		E_m		Unstable	0.024322	0.017333	0.017180
	LQE	E_{ux}		Unstable	0.025654	0.021368	0.025859
		E_{uy}		Unstable	0.026074	0.021697	0.027291
		E_p		Unstable	0.022584	0.013853	0.011115
		E_m		Unstable	0.024771	0.018973	0.021422
160	BGK				Unstable		
	EQE	E_{ux}	0.020997	0.019602	0.017802	0.015361	0.017890
		E_{uy}	0.021505	0.020143	0.018389	0.016036	0.017647
		E_p	0.060736	0.036427	0.016648	0.010302	0.006782
		E_m	0.034413	0.025391	0.017613	0.013899	0.014106
	LQE	E_{ux}	0.021026	0.019723	0.018533	0.017777	0.020943
		E_{uy}	0.021532	0.020251	0.019038	0.018193	0.021381
		E_p	0.060735	0.036431	0.016770	0.010955	0.009773
		E_m	0.034431	0.025468	0.018113	0.015641	0.017365
192	BGK				Unstable		
	EQE	E_{ux}	0.017678	0.016956	0.015552	0.013709	0.017191
		E_{uy}	0.018232	0.017524	0.016141	0.014271	0.016394
		E_p	0.052492	0.029327	0.013544	0.008573	0.005709
		E_m	0.029467	0.021269	0.015079	0.012184	0.013098
	LQE	E_{ux}	0.017710	0.017083	0.016296	0.015929	0.020282
		E_{uy}	0.018260	0.017635	0.016820	0.016423	0.020556
		E_p	0.052491	0.029335	0.013680	0.009226	0.008980
		E_m	0.029487	0.021351	0.015599	0.013859	0.016606
224	BGK				Unstable		
	EQE	E_{ux}	0.016072	0.015457	0.014431	0.012944	0.016608
		E_{uy}	0.016653	0.016004	0.014826	0.013269	0.016008
		E_p	0.045503	0.024187	0.011551	0.007471	0.004960
		E_m	0.026076	0.018549	0.013603	0.011228	0.012525
	LQE	E_{ux}	0.016105	0.015583	0.015152	0.015011	0.019737
		E_{uy}	0.016682	0.016120	0.015555	0.015426	0.019777
		E_p	0.045504	0.024199	0.011690	0.008124	0.008440
		E_m	0.026097	0.018634	0.014132	0.012854	0.015984

TABLE III. (*Continued.*)

			Ma				
1/Kn	Scheme	Error	0.02	0.04	0.10	0.20	0.40
256	BGK	E_{ux}		Unstable		0.014487	0.019473
		E_{uy}		Unstable		0.014560	0.019406
		E_p		Unstable		0.007048	0.007872
		E_m		Unstable		0.012031	0.015583
	EQE	E_{ux}	0.015062	0.014615	0.013801	0.012247	0.016124
		E_{uy}	0.015539	0.014948	0.013954	0.012617	0.015883
		E_p	0.039344	0.020624	0.010162	0.006665	0.004403
		E_m	0.023315	0.016729	0.012639	0.010509	0.012137
	LQE	E_{ux}	0.015094	0.014738	0.014543	0.014439	0.019189
		E_{uy}	0.015570	0.015073	0.014676	0.014592	0.019095
		E_p	0.039345	0.020637	0.010309	0.007368	0.008023
		E_m	0.023336	0.016816	0.013176	0.012133	0.015436

allows one to recover a complete picture of the enhanced numerical stability of the proposed schemes, without neglecting the effects on accuracy as well.

V. CONCLUSIONS

Taking advantage of the analytically generalized Maxwell distribution function, a quasiequilibrium model (EQE) is proposed, which enjoys both the H theorem and the additional free-tunable parameter for controlling the bulk viscosity and enhancing the stability of the model, when the incompressible limit is the only concern. A simpler model based on a proper expansion with regards to the low Mach number limit is derived as well (LQE). Because all the results above are derived in a closed form, numerical implementations of both models is straightforward, is not essentially different from the standard LBGK scheme, and the practical details are reported. Extensive numerical tests concerning the lid driven cavity are considered in order to verify the effective transport coefficients and the enhancement of the stability region.

Since the lid driven cavity test involves a singular pressure field, this test is particularly suitable for checking the stability of a numerical scheme dealing with incompressible limit. We started first by considering some specific features of the flow concerning the main vortexes. It comes out that the proposed EQE model, with a rougher mesh $170^2 \sim 250^2/2$ than that used by the BGK model, can achieve the same accuracy ($2.68\% \sim 2.72\%$) in computing the main vortex locations. This leads to an effective computational speed-up of 2.84 in terms of run time. The results are even more encouraging for the model expanded in the low Mach number limit (LQE). In this test, the LQE model is roughly 50% faster than the EQE model, because the first avoids the cumbersome calculations due to the Cardano formula. Moreover, it is even more accurate than the EQE model ($1.80\% < 2.68\%$) with the same mesh (170×170), because it involves a smaller number of operations and hence it is less effected by the round-off errors. For the previous reasons, the LQE model leads to an effective computational speed-up of 4.37 in terms of run time, with regards to the usual lattice BGK model.

TABLE IV. Lid driven cavity stability and global accuracy test: parameter plane for EQE. The Reynolds number is Re=5000, the kinematic viscosity $\nu=0.0002$ and the bulk viscosity $\xi=0.002$. Different meshes (and consequently different Knudsen numbers) $N=1/\mathrm{Kn}$ and different Mach numbers are considered. The arithmetic average E_m among all global errors is reported and the best results are reported in bold. The label "unstable" means that the calculation could not be performed with that combination of simulation parameters.

	$N=1/\mathrm{Kn}$				
Ma	256	224	192	160	128
0.40	0.015436	0.012525	0.013098	0.014106	**0.017180**
0.20	**0.012133**	**0.011228**	**0.012184**	**0.013899**	0.017333
0.10	0.013176	0.013603	0.015079	0.017613	0.024322
0.04	0.016816	0.018549	0.021269	0.025391	Unstable
0.02	0.023315	0.026076	0.029467	0.034413	Unstable

For investigating systematically these results, an extensive simulation plan has been defined, consisting of five values for the Mach number, five values for the numerical Knudsen number and comparing the standard lattice BGK with the proposed schemes (both EQE and LQE). Moreover the accuracy in recovering the global solution was considered too, by comparing the numerical results with a reference solution obtained by a popular commercial tool. It came out that EQE is characterized by better accuracy in recovering the global solution than LQE and, as expected, the discrepancy between these schemes increases as far as the Mach number increases too. Considering the EQE scheme, it is possible to recover the same mean accuracy of the best lattice BGK simulation ($1/\mathrm{Kn}=256$ and $\mathrm{Ma}=0.20$) by using a rougher mesh with $1/\mathrm{Kn}=192$ and $\mathrm{Ma}=0.20$, which corresponds again roughly to half of the previous mesh. Hence also the systematic simulation plan confirms the previous results about some specific features of the flow.

ACKNOWLEDGMENTS

P.A. acknowledges support of EnerGRID project. I.V.K. acknowledges support of CCEM-CH.

APPENDIX: GENERALIZATION TO 3D CASE BY D3Q27 LATTICES

Since the quasiequilibrium is the product of one-dimensional functions in each direction [18], it is very simple to solve the minimization problem in the 3D case, namely, for the D3Q27 lattice,

$$f_{G(0,0,0)} = \frac{\rho}{c^6}(c^2 - P_{xx})(c^2 - P_{yy})(c^2 - P_{zz}),$$

$$f_{G(\pm1,0,0)} = \frac{\rho}{2c^6}(P_{xx} \pm cu_x)(c^2 - P_{yy})(c^2 - P_{zz}),$$

$$f_{G(0,\pm1,0)} = \frac{\rho}{2c^6}(c^2 - P_{xx})(P_{yy} \pm cu_y)(c^2 - P_{zz}),$$

$$f_{G(0,0,\pm1)} = \frac{\rho}{2c^6}(c^2 - P_{xx})(c^2 - P_{yy})(P_{zz} \pm cu_z),$$

$$f_{G(\pm1,\pm1,0)} = \frac{\rho}{4c^6}(P_{xx} \pm cu_x)(P_{yy} \pm cu_y)(c^2 - P_{zz}),$$

$$f_{G(0,\pm1,\pm1)} = \frac{\rho}{4c^6}(c^2 - P_{xx})(P_{yy} \pm cu_y)(P_{zz} \pm cu_z),$$

$$f_{G(\pm1,0\pm1)} = \frac{\rho}{4c^6}(P_{xx} \pm cu_x)(c^2 - P_{yy})(P_{zz} \pm cu_z),$$

$$f_{G(\pm1,\pm1\pm1)} = \frac{\rho}{8c^6}(P_{xx} \pm cu_x)(P_{yy} \pm cu_y)(P_{zz} \pm cu_z). \tag{A1}$$

In order to ensure the positivity of the latter f_G, it is required that $P \in \Psi$ where $\Psi = \{P : c|u_x| < P_{xx} < c^2, c|u_y| < P_{yy} < c^2, c|u_z| < P_{zz} < c^2\}$ is a convex box in the space of parameters for each velocity $\boldsymbol{u}$. Note that, when setting $\Pi_z = 0$ in the nine populations, $f_{G(0,0,0)}$, $f_{G(\pm1,0,0)}$, $f_{G(0,\pm1,0)}$, and $f_{G(\pm1,\pm1,0)}$ [Eq. (A1)], we obtain the quasiequilibrium on the two-dimensional D2Q9 lattice, given by Eq. (30).

With the help of f_G [Eq. (A1)], let us derive a constrained equilibrium f_C which brings the H-function to a minimum among all the population lists with a fixed trace of the pressure tensor $T(\boldsymbol{P}) = P_{xx} + P_{yy} + P_{zz}$. In terms of the parameter set Ψ, this is equivalent to require that the point $C = (P^C_{xx}, P^C_{yy}, P^C_{zz})$ belongs to a surface portion $\mathbf{A}_T = \{P \in \Psi : P_{xx} + P_{yy} + P_{zz} = T\}$, and the constrained equilibrium C is that minimizing the function H_G [Eq. (4)] on $\mathbf{A}_T$. Since the restriction of a convex function to a line is also convex, the solution to the latter problem exists and is found by

$$\frac{dH_G}{dP_{xx}} = \left[\frac{\partial H_G}{\partial P_{xx}} - \frac{\partial H_G}{\partial P_{zz}}\right]_{P_{zz}=T'-P_{xx}} = 0, \tag{A2}$$

$$\frac{dH_G}{dP_{yy}} = \left[\frac{\partial H_G}{\partial P_{yy}} - \frac{\partial H_G}{\partial P_{zz}}\right]_{P_{zz}=T''-P_{yy}} = 0 \tag{A3}$$

where $T' = T - P_{yy}$ and $T'' = T - P_{xx}$. It is possible to compute each of the partial derivatives involved in the previous expressions by the following rule:

$$\frac{\partial H_G}{\partial P_{\alpha\alpha}} = \frac{\rho}{c^2}\ln\frac{\sqrt{a_-(P_{\alpha\alpha})a_+(P_{\alpha\alpha})}}{a_o(P_{\alpha\alpha})} = \frac{\rho}{c^2}\ln\frac{\sqrt{P^2_{\alpha\alpha} - c^2u^2_\alpha}}{(c^2 - P_{\alpha\alpha})/2}. \tag{A4}$$

Each of Eqs. (A2) and (A3) yields to a cubic equation in terms of the normal stress difference $N' = P^C_{xx} - P^C_{zz}$ and $N'' = P^C_{yy} - P^C_{zz}$ respectively. Each cubic equation admits a solution like that described by Eq. (9). In particular, in the low Mach number limit, as already done in Eq. (32), it is possible to approximate exact solutions by

$$P^C_{xx}(\boldsymbol{u},T) = \frac{(T - P^C_{yy}) + (u_x^2 - u_z^2)}{2} + O(\mathrm{Ma}^4),$$

$$P^C_{yy}(\boldsymbol{u},T) = \frac{(T - P^C_{xx}) + (u_y^2 - u_z^2)}{2} + O(\mathrm{Ma}^4),$$

$$P^C_{zz}(\boldsymbol{u},T) = \frac{(T - P^C_{xx}) - (u_y^2 - u_z^2)}{2} + O(\mathrm{Ma}^4)$$

$$= \frac{(T - P^C_{yy}) - (u_x^2 - u_z^2)}{2} + O(\mathrm{Ma}^4). \tag{A5}$$

Clearly the previous conditions are not linearly independent, or equivalently the rank of the previous system of equations is actually equal to three, and it admits the following solutions:

$$P^C_{\alpha\alpha}(\boldsymbol{u},T) = \frac{T}{3} + u_\alpha^2 - \frac{u_x^2 + u_y^2 + u_z^2}{3} + O(\mathrm{Ma}^4), \tag{A6}$$

which corresponds to Eq. (32) in the two-dimensional case. Further details about the three-dimensional case are reported in Ref. [18].

[1] S. Succi, *The Lattice Boltzmann Equation for Fluid Dynamics and Beyond*, 2nd ed. (Oxford University Press, New York, 2001).
[2] G. R. McNamara and G. Zanetti, Phys. Rev. Lett. **61**, 2332 (1988).
[3] Y. Qian, D. d'Humières, and P. Lallemand, Europhys. Lett. **17**, 479 (1992).
[4] S. Succi, I. V. Karlin, and H. Chen, Rev. Mod. Phys. **74**, 1203 (2002).
[5] I. V. Karlin, A. N. Gorban, S. Succi, and V. Boffi, Phys. Rev. Lett. **81**, 6 (1998).
[6] I. V. Karlin, A. Ferrante, and H. C. Ottinger, Europhys. Lett. **47**, 182 (1999).
[7] S. Ansumali, I. V. Karlin, and H. C. Ottinger, Europhys. Lett. **63**, 798 (2003).
[8] S. Ansumali, S. Arcidiacono, S. S. Chikatamarla, N. I. Prasianakis, A. N. Gorban, and I. V. Karlin, Eur. Phys. J. B **56**, 135 (2007).
[9] S. S. Chikatamarla and I. V. Karlin, Phys. Rev. Lett. **97**, 190601 (2006).
[10] F. Higuera, S. Succi, and R. Benzi, Europhys. Lett. **9**, 345 (1989).
[11] D. d'Humières, Prog. Astronaut. Aeronaut. **159**, 450 (1992).
[12] P. Lallemand and L.-S. Luo, Phys. Rev. E **61**, 6546 (2000).
[13] P. Asinari, Phys. Rev. E **78**, 016701 (2008).
[14] P. Asinari and I. V. Karlin, Phys. Rev. E **79**, 036703 (2009).
[15] A. Gorban and I. Karlin, Physica A **206**, 401 (1994).
[16] C. Levermore, J. Stat. Phys. **83**, 1021 (1996).
[17] B. M. Boghosian, J. Yepez, P. V. Coveney, and A. Wager, Proc. R. Soc. London, Ser. A **457**, 717 (2001).
[18] I. Karlin and P. Asinari, Physica A (to be published).
[19] X. Shan and X. He, Phys. Rev. Lett. **80**, 65 (1998).
[20] A. N. Gorban and I. V. Karlin, *Invariant Manifolds for Physical and Chemical Kinetics, no. 660 in Lecture Notes in Physics*, 1st ed. (Springer-Verlag, Berlin, 2005).
[21] N. I. Prasianakis, I. V. Karlin, J. Mantzaras, and K. B. Boulouchos, Phys. Rev. E **79**, 066702 (2009).
[22] M. Junk, A. Klar, and L.-S. Luo, J. Comput. Phys. **210**, 676 (2005).
[23] X. He, S. Chen, and G. Doolen, J. Comput. Phys. **146**, 282 (1998).
[24] P. Asinari and T. Ohwada, Comput. Math. Appl. **58**, 841 (2009).
[25] U. Ghia, K. Ghia, and C. Shin, J. Computat. Phys. **48**, 387 (1982).
[26] R. Schreiber and H. Keller, J. Comput. Phys. **49**, 310 (1983).
[27] S. P. Vanka, J. Comput. Phys. **65**, 138 (1986).
[28] S. L. Hou, Q. Zou, S. Chen, G. D. Doolen, and A. C. Cogley, J. Comput. Phys. **118**, 329 (1995).
[29] S. Ansumali and I. V. Karlin, Phys. Rev. E **66**, 026311 (2002).
[30] S. Patankar, *Numerical Heat Transfer and Fluid Flow*, 1st ed. (Hemisphere Publishing Corporation, USA, 1980).